Energies **2015**, *8*, 10389-10408; doi:10.3390/en80910389

OPEN ACCESS

energies

ISSN 1996-1073

www.mdpi.com/journal/energies

Article

Real-Time Control of Active and Reactive Power for Doubly Fed Induction Generator (DFIG)-Based Wind Energy Conversion System

Aman Abdulla Tanvir [1,*], Adel Merabet [1] and Rachid Beguenane [2]

[1] Division of Engineering, Saint Mary's University, Halifax B3H 3C3, NS, Canada; E-Mail: adel.merabet@smu.ca

[2] Department of Electrical and Computer Engineering, Royal Military College, Kingston K7K 7B4, ON, Canada; E-Mail: rachid.beguenane@rmc.ca

* Author to whom correspondence should be addressed; E-Mail: aman.tanvir@smu.ca; Tel.: +1-902-420-5101; Fax: +1-902-420-5021.

Academic Editor: Frede Blaabjerg

Received: 13 July 2015 / Accepted: 15 September 2015 / Published: 21 September 2015

Abstract: This paper presents the modeling, rapid control prototyping, and hardware-in-the-loop testing for real-time simulation and control of a grid-connected doubly fed induction generator (DFIG) in a laboratory-size wind turbine emulator for wind energy conversion systems. The generator is modeled using the direct-quadrature rotating reference frame circuit along with the aligned stator flux, and the field-oriented control approach is applied for independent control of the active and reactive power and the DC-link voltage at the grid side. The control of the active, reactive power and the DC-link voltage are performed using a back-to-back converter at sub- and super-synchronous as well as at variable speeds. The control strategy is experimentally validated on an emulated wind turbine driven by the Opal-RT real-time simulator (OP5600) for simultaneous control of the DC-link voltage, active and reactive power.

Keywords: doubly fed induction generator; wind energy conversion system; field oriented control; rapid control prototyping; hardware-in-the-loop

---

1. Introduction

The future trend of energy production is moving towards a higher share of renewable energy sources driven by global warming issues and the desire to reduce dependence on fossil fuels. Wind power generation is one of the most attractive of the renewable energy sources due to its availability in different areas and the economic benefits of generating large-scale power. So, the dependency on large-scale wind turbines or wind farms is increasing day by day for power generation [1]. A doubly fed induction generator (DFIG) is one of the most widely used generators in wind turbines due to its variable speed operation, power control, improving power quality, smaller converter capacity, and grid tie feasibility. The DFIG is able to control its active and reactive power outputs as required by system operators. Although the active power depends on the energy transferred from the wind, it can be controlled in a transient manner by resorting to the mechanical system kinetic energy. This will allow more renewable energy resources with DFIG as a combined system to be connected to the grid. When two or more renewable energy resources generate maximum power by controlling the active power of DFIG, the total system power can be controlled to fulfill the grid requirement. In the case of a weak grid, where the voltage may fluctuate, the DFIG may be ordered to produce or absorb an amount of reactive power to or from the grid, with the purpose of voltage control. Therefore, the control technologies and the dynamic characteristics of the variable-speed constant-frequency (VSCF) doubly fed induction generator are important topics in wind energy research [2].

In doubly-fed configuration, two back-to-back connected converters provide the required magnetization current at rotor windings. In fact, three phase power supply or grid connection to a three phase converter provides a stable DC-link voltage. This converter is usually called grid side converter (GSC). The DC-link voltage can be used as the voltage source for the other three phase converters, which are directly connected to the rotor winding terminals and called rotor side converters (RSC).

Although the main task of GSC is to keep the DC-link voltage constant, it may also be used to compensate for the reactive power or in some cases to remove the reactive power pulsation during unbalanced conditions [3]. The RSC would provide the required magnetization current waveforms in rotor windings to generate the required active and reactive power at stator terminals.

According to a survey done by O. Carlson *et al.* [4], the energy production can be increased by 2%–6% for a variable-speed wind turbine in comparison to a fixed-speed wind turbine, while D.S. Zinger *et al.* [5] stated that the increase in energy can be 39%. German brochure *et al.* [6] shows that the gain in energy generation of the variable-speed wind turbine compared to the most simple fixed-speed wind turbine can vary between 3%–28% depending on the site conditions and design parameters. Calculations of the energy efficiency of the doubly-fed induction generator system have been presented in several papers [7–9]. A comparison to other electrical systems for wind turbines is, however, harder to find. R. Datta *et al.* [10] have made a comparison of the energy capture for different schemes of the electrical configuration, *i.e.*, a fixed-speed wind turbine using an induction generator, full variable-speed wind turbine using an inverter-fed induction generator, and a variable-speed wind turbine using a doubly-fed induction generator. The energy capture can be significantly enhanced by using a doubly-fed induction machine as a generator and the increased energy capture of a doubly-fed induction generator by over 20% with respect to a variable-speed system using a cage rotor induction machine and

by over 60% in comparison to a fixed-speed system [10]. Aspects such as the wind distribution and electrical and mechanical losses in the systems were neglected in that study. When the doubly fed generation method was introduced and implemented for reluctance machines [11], the idea led to early attempts to use wound rotor induction machines for such applications. The first implementation of DFIG is recorded by R. Pena *et al.* [12], where the control strategy is based on PI controllers in conjunction with a sinusoidal PWM that ends up with a constant switching frequency. This work was followed by more research in control method. The detailed model-based studies on DFIG are presented by R. Pena, where the rotor position would be found through current and voltage models [13]. Another important modeling study is reported by A. Peterson *et al.* [14], namely the grid integration of the DFIG and its operation under voltage sag. Further studies on transient analysis of doubly fed induction generator followed in P. Ledesma *et al* [15]. Implementation of the current controlled method on DFIG using hysteresis controller to achieve better dynamics was reported by Chowdhury *et al.* [16]. To study the DFIG, RSC and GSC might be studied separately. In practice, as long as a stable DC-link voltage is provided by GSC, the RSC can operate in total isolation from the GSC. M. Mesbah *et al.* [17] provides a GSC that is able to control the DC-link voltage even in unbalanced grid voltage source condition. However, the solution lacks the reactive power compensation. Also, in most methods, RSC operates in total isolation from the GSC and a separate controller would handle the operation of each converter. On the other hand, to deal with the active power pulsations in an unbalanced grid voltage, there is a control method reported in L. Xu *et al.* [3], where both converters are considered in one control loop. Thus, the set points of GSC would be derived out of the RSC set points and the turbine generator operating condition. A feedback linearization based nonlinear voltage and slip controller are proposed by A. Balogun *et al.* [18] for a DFIG connected to an infinite bus. A direct active and reactive power controller based on stator flux estimation is discussed by B. Singh *et al.* [19]. The paper uses a basic hysteresis controller. M.E. Zarei *et al.* [20] proposed the well-known vector control and direct power control to regulate the active and reactive power generated by DFIG. A DFIG control strategy that is very similar to the conventional AVR/PSS for synchronous generator is proposed by R.Dev Shukla *et al.* [21] to support the power grid voltage and frequency.

Several researchers are still investigating the best control strategies to improve the performance of DFIG [22], which is a key concern for DFIG. The main drawback of these works is their inability to cope with large changes in grid parameters. Furthermore, in B. Singh *et al.* [19], the rotor position is estimated using stator voltage-current and rotor current, where the rotor is connected to a battery bank with a fixed DC-link voltage producing a fixed rotor current, which is not economical and applicable in large-scale wind farms as the rotor is connected to the grid through a DC-link converter and its voltage needs to be regulated to overcome the variations in the system, and in [23], the vector control and direct power controller for the rotor side converter is applied without any control for the DC-link voltage, which is an important issue for the practical operation of DFIG based Wind Energy Conversion System (WECS). Even though practical results from the previous studies have offered some useful hints for hardware setup, there is not enough detailed design available in the literature. For this reason, the study of DFIG through a practical implementation would help to justify various methods and ideas that will be investigated in this work.

This paper proposes a theoretical and physical implementation of a control scheme for the Double Fed Induction Generator based Wind Turbine (DFIG-WT). The control design uses the field-oriented

control (FOC) theory to regulate the rotor side converter (RSC) and the hysteresis control approach to regulate the grid side converter (GSC). The most challenging task in DFIG operation is to keep the DC-link voltage constant. In this paper, a hysteresis controller is developed for the voltage side controller, which has a fast dynamic response. The traditional current control strategies are mostly proportional-integral (PI) based on a linearized model; they are difficult to obtain and may not give satisfactory performance under parameter variations, load disturbances, and a large-scale wind changes. The RSC control scheme leads to an independent control of the DFIG active and reactive power by controlling the rotor currents. For its implementation, this type of control heavily relies on the electrical parameters of the machine and multiple reference frame transformations of the electrical signals (voltages and currents). However, the FOC approach delivers a great control performance in terms of robustness, transitory and steady state response, and instrumentation specifications. The grid side converter (GSC) facilitates the power exchange through the rotor converter, and also provides additional reactive power support. GSC is controlled by a hysteresis current controller in such a way as to guarantee a smooth DC-link voltage and ensure sinusoidal current in the grid side. This paper investigates DFIG power generation and converter control characteristics through a dynamic steady-state approach, which provides better and effective understanding of DFIG in wind energy applications under different control conditions in a broader spectrum.

In order to show the performance of the control scheme, an experimental platform has been designed and used. It consists of the LabVolt 2 kW DFIG system with OPAL-RT's OP5600/8660 Real-Time HIL Controller and Data Acquisition System. The control algorithms are carried out by the Opal-RT's powerful real-time target simulator equipped with 3.3-GHz processor core and implemented in Matlab/Simulink and RT-LAB software.

2. System Modeling

2.1. Wind Turbine

Wind turbines produce electricity by using the power of the wind to drive an electrical generator. Wind passes over the blades, generating lift and exerting a turning force. The rotating blades turn a shaft inside the nacelle, which goes into a gearbox. The gearbox increases the rotational speed to that which is appropriate for the generator, which uses magnetic fields to convert the rotational energy into electrical energy.

The expression of power produced by the wind is given by [19]:

$$P_m = 0.5C_p(\lambda, \beta)\rho\pi r^2 v^3 \quad (1)$$

where ρ is the air density; r is the radius of the turbine blades, v is the wind speed, and C_p is the power coefficient, which is a function of tip speed ratio λ and pitch angle β.

The tip speed ratio is defined as:

$$\lambda = \frac{\omega r}{v} \quad (2)$$

where ω is the rotational speed of generator.

From Equation (2), it can be observed that the tip speed ratio λ can be adjusted by controlling the speed ω, leading to the control of the power coefficient C_p, as well as the generated output power of the wind turbine.

In this work, a dynamometer, based on a squirrel cage induction motor, is used to emulate the wind turbine by changing its speed to produce the variable wind speed effects.

2.2. Modeling of Doubly Fed Induction Machine (DFIM)

The DFIG can be regarded as a traditional induction generator with a nonzero rotor voltage. The dynamic equation of a three-phase DFIG can be written in a synchronously rotating direct-quadrature (*d*-*q*) reference frame as [24]:

$$v_{ds} = R_s i_{ds} - \omega_s \psi_{qs} + \frac{d\psi_{ds}}{dt} \quad (3.a)$$

$$v_{qs} = R_s i_{qs} + \omega_s \psi_{ds} + \frac{d\psi_{qs}}{dt} \quad (3.b)$$

$$v_{dr} = R_r i_{dr} - s\omega_s \psi_{qr} + \frac{d\psi_{dr}}{dt} \quad (4.a)$$

$$v_{qr} = R_r i_{qr} + s\omega_s \psi_{dr} + \frac{d\psi_{qr}}{dt} \quad (4.b)$$

$$\psi_{ds} = L_s i_{ds} + L_m i_{dr} \quad (5.a)$$

$$\psi_{qs} = L_s i_{qs} + L_m i_{qr} \quad (5.b)$$

$$\psi_{dr} = L_r i_{dr} + L_m i_{ds} \quad (6.a)$$

$$\psi_{qr} = L_r i_{qr} + L_m i_{qs} \quad (6.b)$$

where ω_s is the rotational speed of the synchronous reference frame; $s\omega_s = (\omega_s - \omega_e)$ is the slip frequency and s is the slip; ω_e is the generator electrical speed, which is related to the generator mechanical speed by mean of the pole numbers $\omega_e = \frac{P}{2}\omega_r$,$R_s$, R_r, L_s and L_r are the stator and rotor resistances and inductances; L_m is the mutual inductance; and ω_r is the angular rotor speed.

The produced electrical torque from the DFIG can be calculated by:

$$T_e = \frac{3}{2}P(\psi_{dr} i_{qs} - \psi_{qr} i_{ds}) = \frac{3}{2}PL_m(i_{dr} i_{qs} - i_{qr} i_{ds}) \quad (7)$$

where P is the pole numbers and $L_M = {}^3/_2\, L_m$.

The active and reactive stator and rotor powers for the DFIG are given by:

$$P_s = \frac{3}{2}(v_{ds} i_{ds} + v_{qs} i_{qs}) \quad (8)$$

$$Q_s = \frac{3}{2}(v_{qs} i_{ds} - v_{ds} i_{qs}) \quad (9)$$

$$P_r = \frac{3}{2}(v_{dr} i_{dr} + v_{qr} i_{qr}) \quad (10)$$

$$Q_r = \frac{3}{2}(v_{qr} i_{dr} - v_{dr} i_{qr}) \quad (11)$$

where the power losses associated with the stator and rotor resistances are neglected.

3. Control Strategy of Doubly Fed Induction Generator

The DFIG control comprises both the rotor side converter (RSC) and the grid side converter (GSC) controllers so that the RSC controls active and reactive power [25] and the GSC regulates the DC-link voltage as well as generates an independent reactive power that is injected into the grid.

3.1. Grid Side Controller

The main objective of the grid side controller is to keep a constant DC-link voltage independent of the value and direction of the rotor power flow [12]. To fulfill the objective, a hysteresis current control strategy with a reference frame aligned with the stator voltage position is used as shown in Figure 1. This allows independent control of the DC-link voltage and the reactive power between the converter and the grid.

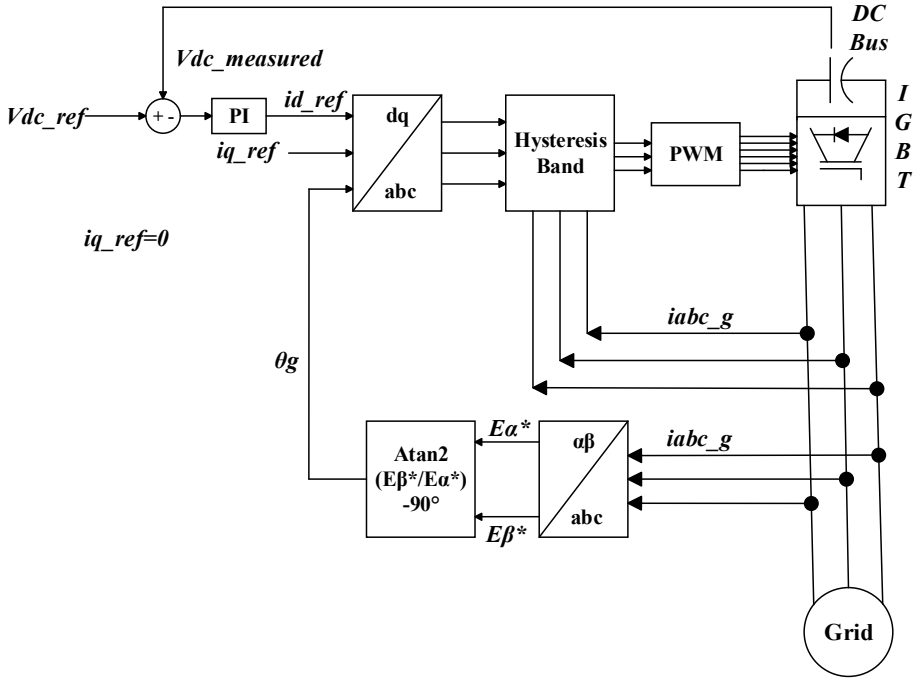

Figure 1. The block diagram of proposed method for GSC.

The rotor side converter requires a DC power supply. The DC voltage is usually generated using another voltage source converter connected to the AC grid at the generator stator terminals. A DC capacitor is used in order to remove ripple and keep the DC-link voltage relatively smooth. This grid PWM converter is operated to keep the DC-link voltage at a constant value. In effect, this means that the grid side converter is supplying the real power demands of the rotor side converter. It is possible to operate this converter using a current reference approach. Therefore, a hysteresis controller is used in which the error between the desired and actual currents is passed through a controller, which controls the output voltage of a conventional Sinusoidal PWM Converter and ensures the required power factor [26]. The grid side converter control diagram is shown in Figure 1.

The DC-link voltage error is given by:

$$e = v_{dc\_ref} - v_{dc} \tag{12}$$

Also, its variation is expressed by:

$$\Delta e = (1 - z^{-1}) \tag{13}$$

The voltage components, in the (d-q) rotating reference frame, at the grid side are given by:

$$v_d = Ri_d + L\frac{di_d}{dt} - L\omega i_q + v_{dl} \tag{14}$$

$$v_q = Ri_q + L\frac{di_q}{dt} + L\omega i_d + v_{ql} \tag{15}$$

where v_d, v_q are the grid voltage (d-q) components; v_{dl}, v_{ql} are the grid inverter voltage (d-q) components; i_d, i_q are the grid current (d-q) components; L and R are the inductance and resistance of the filter; and ω is the grid angular frequency.

The active and reactive power flows are then:

$$P = 3(v_d i_d + v_q i_q) \tag{16}$$

$$Q = 3(v_d i_q - v_q i_d) \tag{17}$$

The detection of the reference angular position of the grid voltage is computed as

$$\theta_e = \int \omega_e \, dt = \tan^{-1}\left(\frac{v_\beta}{v_\alpha}\right) \tag{18}$$

where v_α and v_β are the (α-β) components of the grid voltage. Aligning with the d-component of the voltage v_d makes $v_q = 0$. Also, since the grid voltage has constant amplitude, v_d also has constant amplitude.

The active power, to balance at the DC-link, can be expressed by (neglecting harmonics):

$$v_{dc} i_{os} = 3 v_d i_d \tag{19}$$

The DC-link voltage v_{dc} is controlled by the current i_d in the voltage vector-oriented reference frame. Thus, a reference current i_{d_ref} is derived from the DC-link voltage error Δe and the variation of the error e by tuning a PI controller, as shown in Figure 1. To guarantee a unity factor power at the grid side converter, the reactive power must be zero, so $i_{q_{ref}} = 0$. After a *dq-abc* transformation of these reference currents, hysteresis modulation may then be implemented.

3.2. Machine Side Controller

The doubly fed induction generator allows power output into the stator winding as well as the rotor winding of an induction machine with a wound rotor winding. Using such a generator, it is possible to get a good power factor even when the machine speed is quite different from the synchronous speed. Such machines can therefore operate without the need for excessive shunt compensation.

The rotor currents i_{abc_r} of the machine can be resolved into the (d-q) components i_{dr} and i_{qr}. The component i_{dr} produces a flux in the air gap, which is aligned with the rotating flux vector linking the stator, whereas the component i_{qr} produces flux at right angles to this vector. The torque in the machine is the vector cross product of these two vectors, and hence only the component i_{qr} contributes to the machine torque and thus to the power. The component i_{dr} then controls the reactive power entering the machine. The precise control of the currents i_{dr} and i_{qr} allows the control of the stator side real and reactive powers.

The important step is to obtain the instantaneous position of the rotating flux vector in space in order to obtain the rotating reference frame. This can be achieved by realizing that, on account of Lenz's law of electromagnetism, the stator voltage is simply the derivative of the stator flux linkage.

The three phase stator voltages and currents are converted into the (α-β) components v_α, v_β, i_α and i_β. The stator flux in the stationary (α-β) reference frame is given by:

$$\psi_{\alpha\beta s} = \int v_{\alpha\beta s} - R_s i_{\alpha\beta s} dt = (\psi_{\alpha s}, \psi_{\beta s}) \tag{20}$$

In order to align the synchronously rotating (*d*-*q*) reference frame with the stator flux, information about the angle stator flux can be extracted using the following expressions:

$$\psi_s = |\psi_{\alpha\beta s}| angle(\psi_{\alpha\beta s}) \tag{21}$$

$$angle(\psi_{\alpha\beta s}) = \theta_s = \tan^{-1}(\psi_{\alpha s} / \psi_{\beta s});\ |\psi_{\alpha\beta s}| = \sqrt{{\psi_{\alpha s}}^2 + {\psi_{\beta s}}^2} \tag{22}$$

The angle θ_s gives the instantaneous location of the stator's rotating magnetic field. The rotor itself is rotating and is instantaneously located at angle θ_r. Thus, with a reference frame attached to the rotor, the stator's magnetic field vector is at the location $\theta_s - \theta_r$, which is referred to as the "slip angle".

From Equations (3.a)–(3.b), the alignment of the reference frame leads to a simplified model:

$$v_{qs} = \omega_s \psi_{ds} = v_s;\ v_{ds} = 0 \tag{23}$$

It can be observed that the electromagnetic torque depends on the i_{qr} current and can be controlled by the v'_{qr}. Also, the rotor magnetizing current i_{dr} can be controlled by the v'_{dr} voltage component. The controller is shown in Figure 2, where the errors between the currents i_{dr} and i_{qr} and the reference currents i_{dr_ref} and i_{qr_ref} are applied to the PI controllers to obtain the voltages v'_{dr} and v'_{qr} respectively. The controller output should be compensated with two decoupling terms in order to get the appropriate reference voltages, v_{dr_ref} and v_{qr_ref} as follows:

$$v_{dr\_ref} = R_r i_{dr} + \sigma L_r \frac{di_{dr}}{dt} - \omega_{slip} \sigma L_r i_{qr} \tag{24}$$

$$v_{qr\_ref} = R_r i_{qr} + \sigma L_r \frac{di_{qr}}{dt} + \omega_{slip}(\frac{L_m}{L_s}\psi_{ds} + \sigma L_r i_{dr}) \tag{25}$$

where, $\psi_{ds} = \psi_s = L_M I_{ms};\ I_{ms} = \psi_{ds} / L_M;\ \psi_{dr} = {L^2}_M I_{ms} / L_s + \sigma L_r i_{dr};\ \psi_{qr} = \sigma L_r i_{qr};$ $\omega_{slip} = \omega_s - \omega_r;\ \sigma = 1 - \frac{{L_M}^2}{L_s L_r}$.

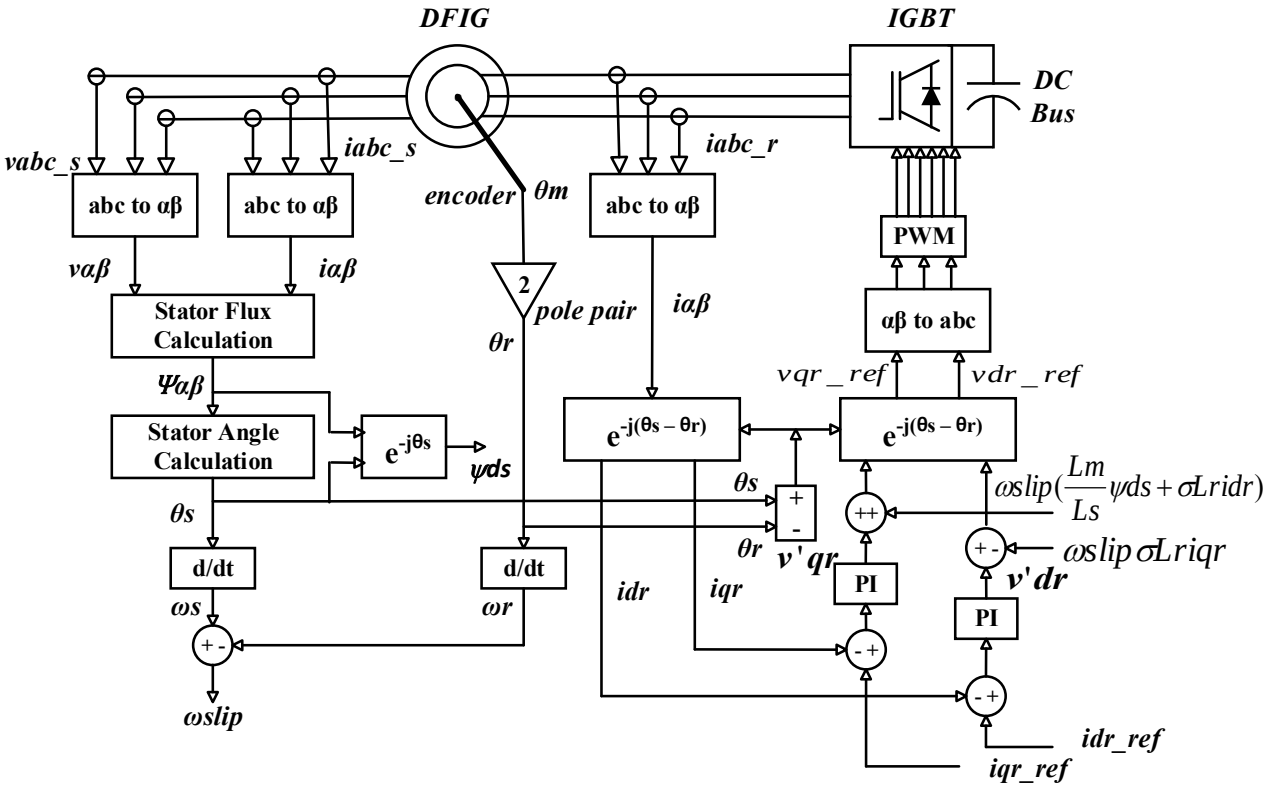

Figure 2. Control algorithm for the the DFIG-based WECS.

In this control approach, both rotor currents (i_{dr}, i_{qr}) are to be controlled in order to follow their respective references, i_{dr_ref} and i_{qr_ref}. Given the alignment of the reference frame with the stator flux, the *q*-current controls the active power of the machine whereas the direct current controls its reactive power. Thus, the *q*-current can be related to the electrical torque of the machine and the *d*-current can be related to the voltage value at the Point of Common Coupling (PCC) as indicated by:

$$i_{dr\_ref} = v_{qs}/\omega_s L_M \tag{26}$$

$$i_{qr\_ref} = -2T_e L_s/(3PL^2{}_M i^*{}_d). \tag{27}$$

The PWM converter acts on the rotor of the generator and the control is done by means of the signals of the rotor and the stator currents, the stator voltage, and the rotor position [23].

4. Experimental Results

The experimental system shown in Figure 3 consists of a doubly fed induction generator, dynamometer, IGBT inverters, line inductors, power supply, Opal RT's data acquisition system OP8600, and real-time digital simulator OP5600, which is a powerful tool for rapid control prototyping with a processor Intel Xeon Quad Core 2.4 GHz. The system parameters are listed in Table A1 (see the appendix). The schematic of all connected modules is shown in Figure 4.

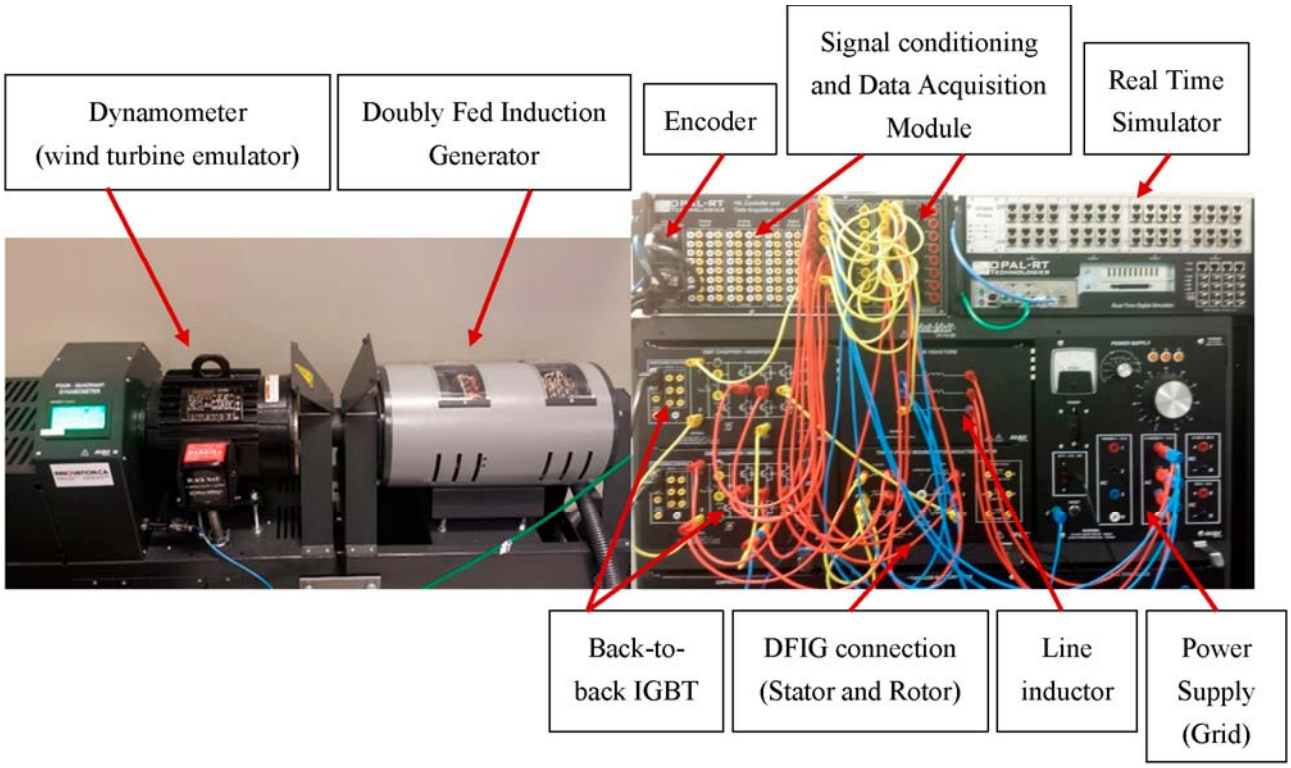

Figure 3. Experimental setup to emulate WECS.

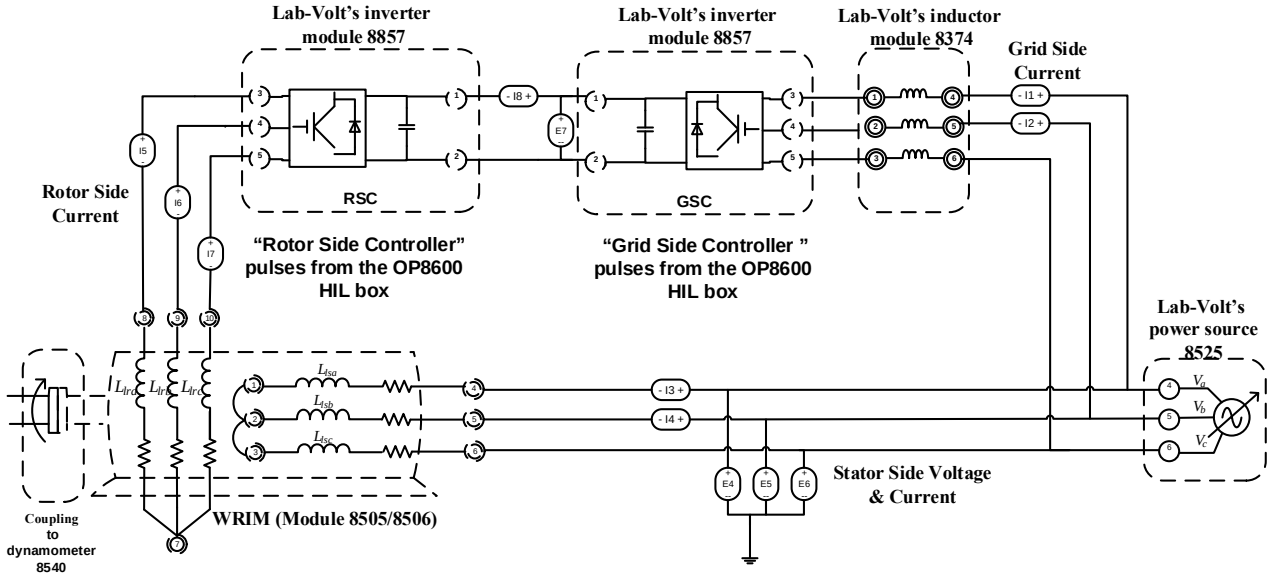

Figure 4. Schematic of the connected experimental setup to emulate WECS.

The four-quadrant dynamometer, a type of squirrel cage induction motor, works as a real wind turbine emulator by running at a variable speed to generate the effect of wind on the bladed rotor of a wind turbine.

Following Equations (10) and (11), the active and reactive powers can be manipulated by controlling the rotor currents through the machine side controller. Furthermore, a proper power transfer can be ensured by regulating the DC-link voltage using the grid side controller. Several experiments are carried out in order to demonstrate the capabilities of the control system to operate the wind energy conversion under different scenarios of power extraction and transfer.

4.1. Power Control by Rotor D-Current

In this test, the dynamometer (wind turbine emulator) is running at constant speed, as shown in Figure 5, and the active and reactive power can be controlled by controlling the rotor *d*-current i_{dr} to follow a reference i_{dr_ref}, while regulating the rotor *q*-current i_{qr} to be constant at i_{qr_ref}. Responses of the controlled rotor *d*- and *q*-currents are illustrated in Figures 6 and 7, respectively, and it can be seen that the current tracking for both currents is successfully achieved. From the power response, shown in Figure 8, it can be observed that the active and reactive power can be controlled by varying the rotor *d*-current i_{dr_ref}. The reactive power increases while the active power decreases to balance the total power. This is a practical controller that supports the reactive power to the grid to improve the power factor. Furthermore, the DC-link voltage is successfully regulated to follow a constant reference, as shown in Figure 9, by the grid side controller despite the variation of the rotor *d*-current at the machine side.

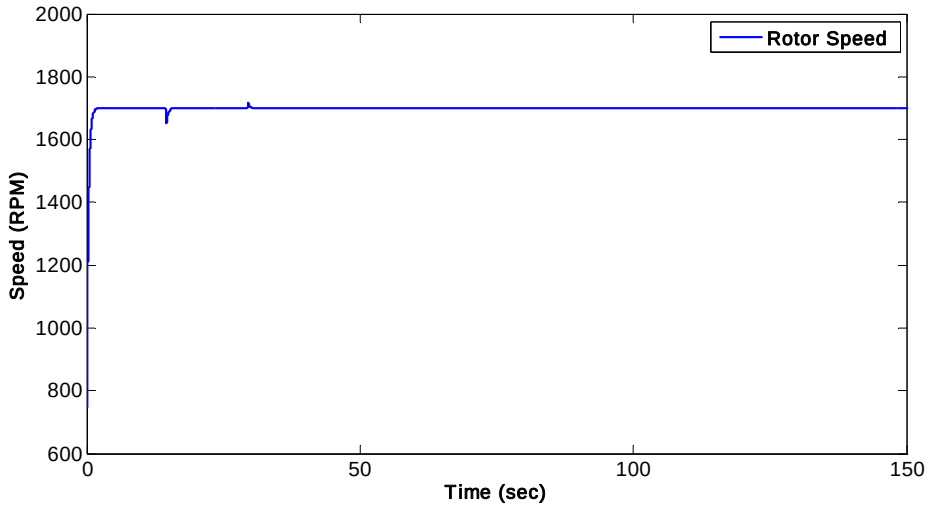

Figure 5. Rotor speed of DFIG.

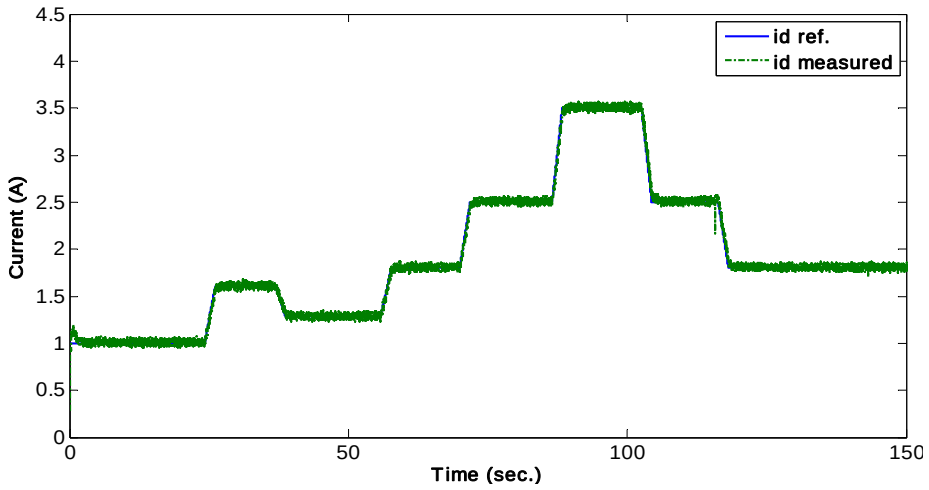

Figure 6. Response of the controlled rotor *d*-current.

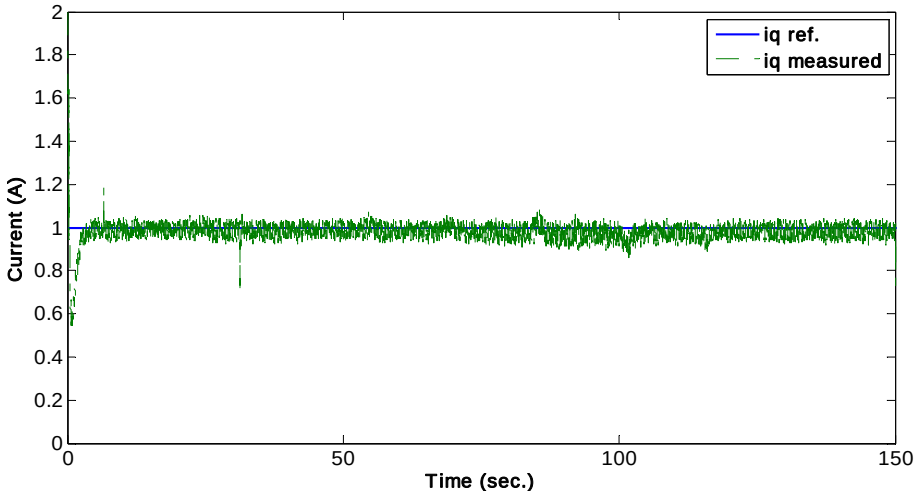

Figure 7. Response of the controlled rotor *q*-current.

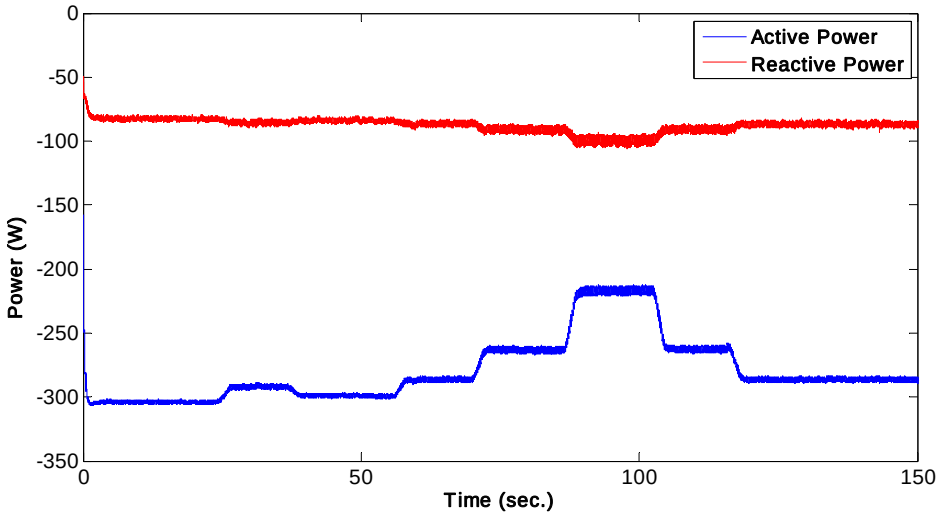

Figure 8. Power response by varying the rotor *d*-current.

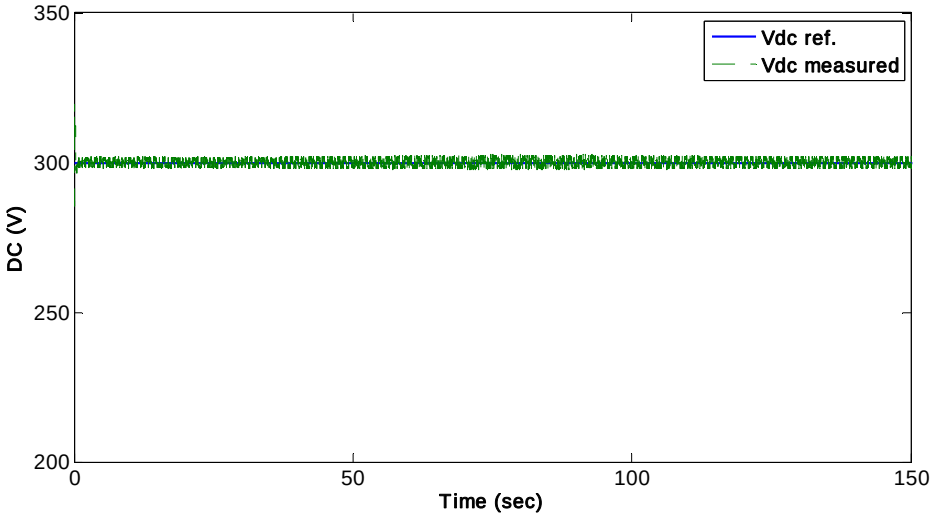

Figure 9. DC-link voltage regulation.

4.2. Power Control by Rotor Q-Current

Now, the active and reactive powers can be controlled by controlling the rotor *q*-current i_{qr} to follow a reference i_{qr_ref}, while regulating the rotor *d*-current i_{dr} to be constant at i_{dr_ref} as shown in Figures 10 and 11, respectively. It can be observed that the current tracking performance is good. From the power response, shown in Figure 12, it can be observed that the active power can be varied by controlling the rotor *q*-current to follow a reference i_{qr_ref} equivalent to the desired active power, while the reactive power increases to balance the power with the grid.

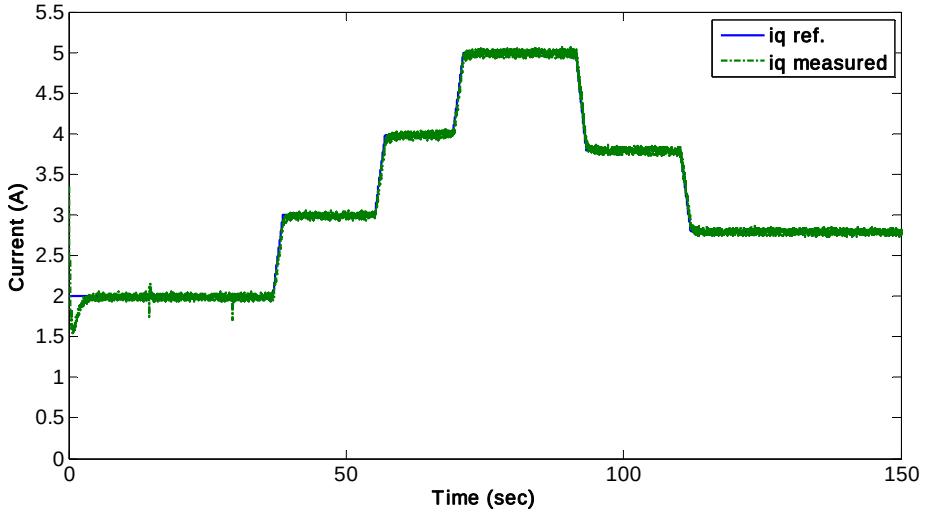

Figure 10. Response of the controlled rotor *q*-current.

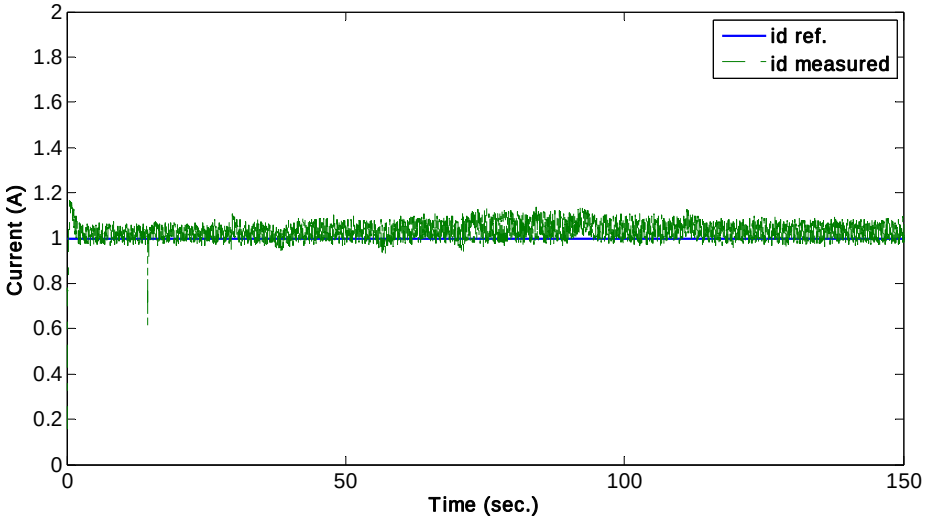

Figure 11. Response of the controlled rotor *d*-current.

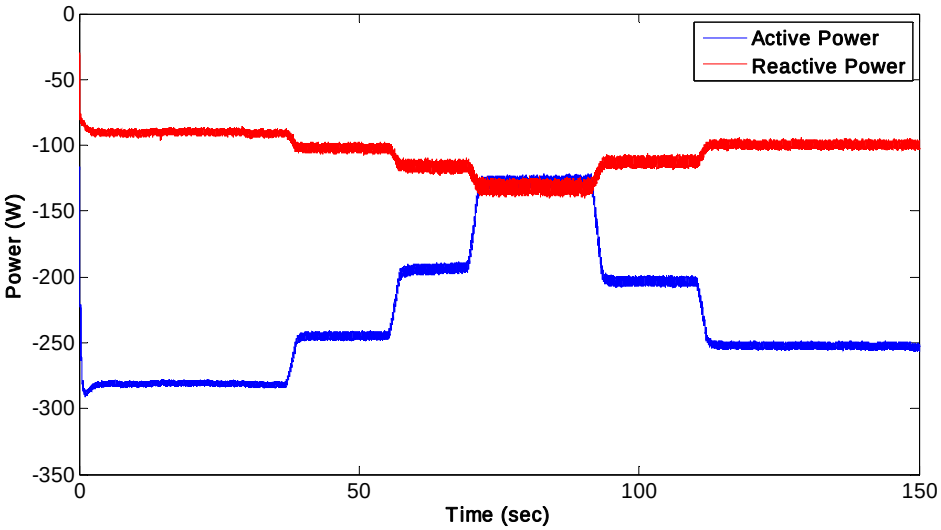

Figure 12. Power response by varying the rotor *q*-current.

4.3. Effect of the DC-Link Voltage Variation on the Rotor Current Control

In this section, the effect of a variable DC-link voltage on the performance of the RSC current controllers is tested. The DC-link voltage is controlled to follow a varying reference, as shown in Figure 13, at the grid side, while the *d*-*q* currents are controlled to track the desired references, as shown in Figures 14 and 15, at the machine side simultaneously. It can be observed that the current tracking performance is well established despite the variation of the DC-link voltage, which ensures the high tracking performance of the overall control system at the grid and machine sides.

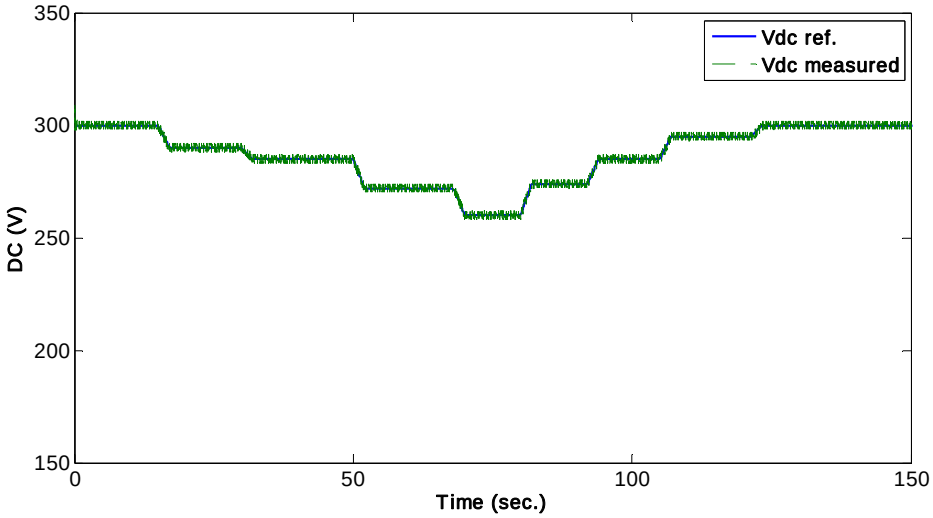

Figure 13. Response of the DC-link voltage controller.

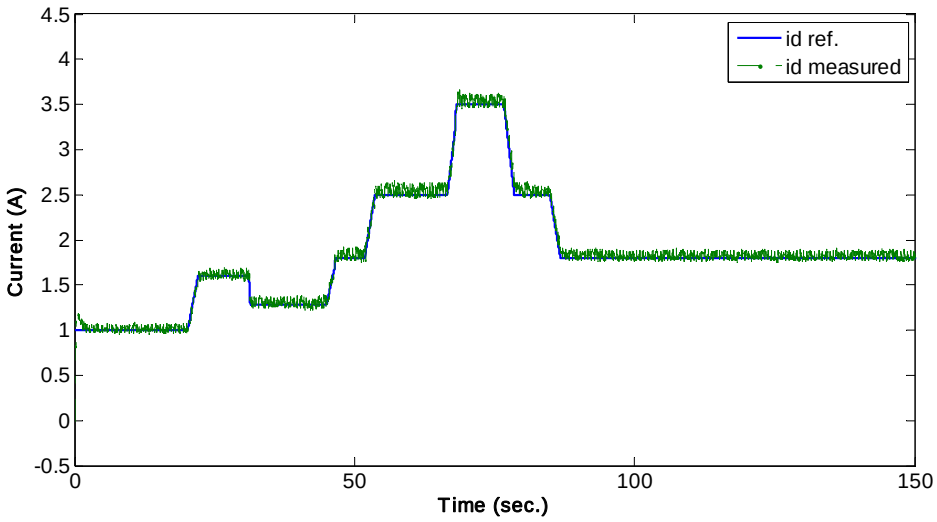

Figure 14. Response of the controlled rotor *d*-current.

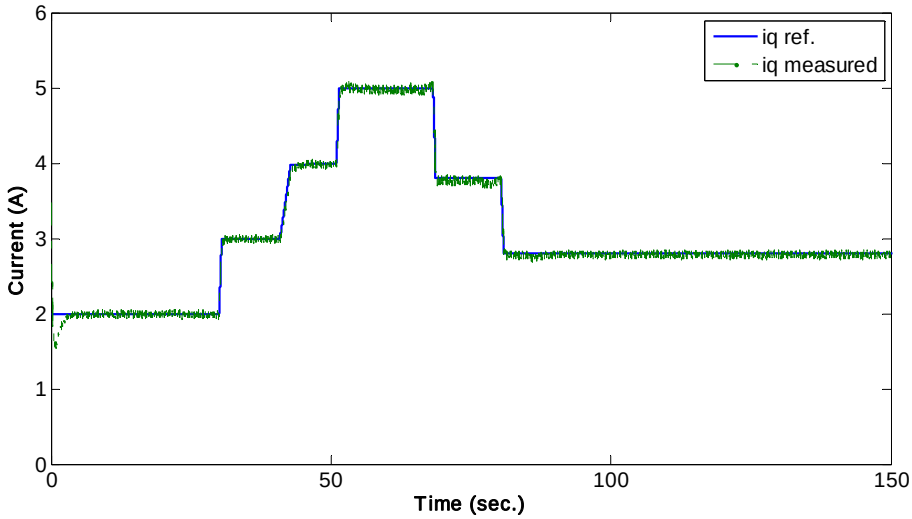

Figure 15. Response of the controlled rotor *q*-current.

4.4. Effects of Variable Rotor Speed on the Rotor Current Control

Finally, the effect of wind speed variation, emulated by varying the rotor speed through the dynamometer, on the rotor *d*-*q* currents is tested by regulating the currents to follow constant references while changing the rotor speed as shown in Figure 16. It can be observed from the *d*-*q* current responses, shown in Figures 17 and 18, that the *d*-current component is well regulated with no effects from the rotor speed variation and the *q*-current component is affected by the rotor speed; however a zero-steady state tracking error is quickly established, which ensures the robustness of the control system. The response for active and reactive power is shown in Figure 19 and it can be observed that they follow the controlled *d*-*q* rotor currents. Therefore, the rotor side controller can be used to regulate the power by tracking appropriate rotor currents. This experiment demonstrates that the power can be controlled to track a desired reference despite the variation of the rotor speed during variable wind speeds.

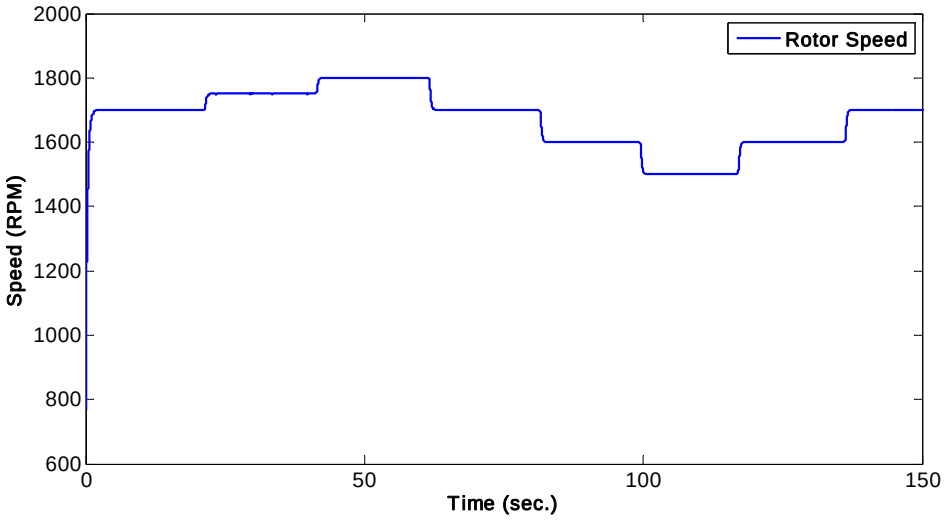

Figure 16. Variable rotor speed of DFIG.

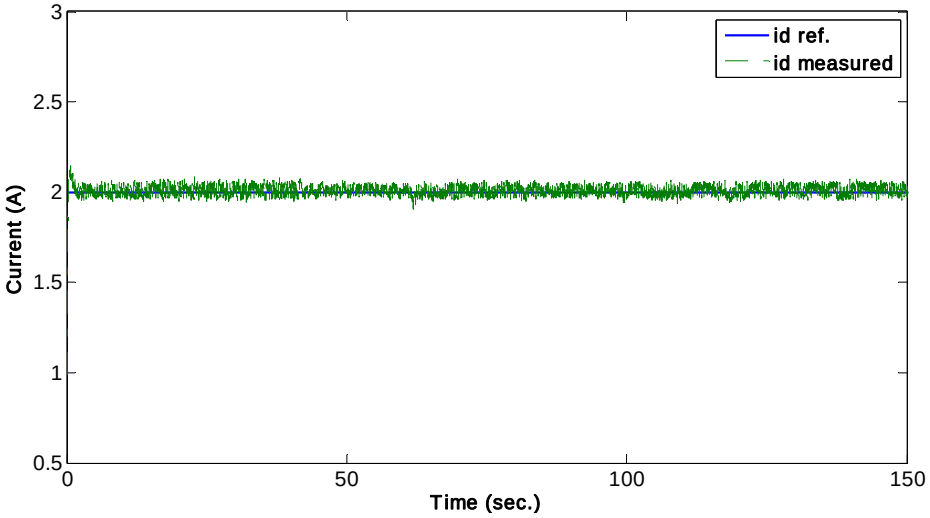

Figure 17. Response of the controlled rotor *d*-current.

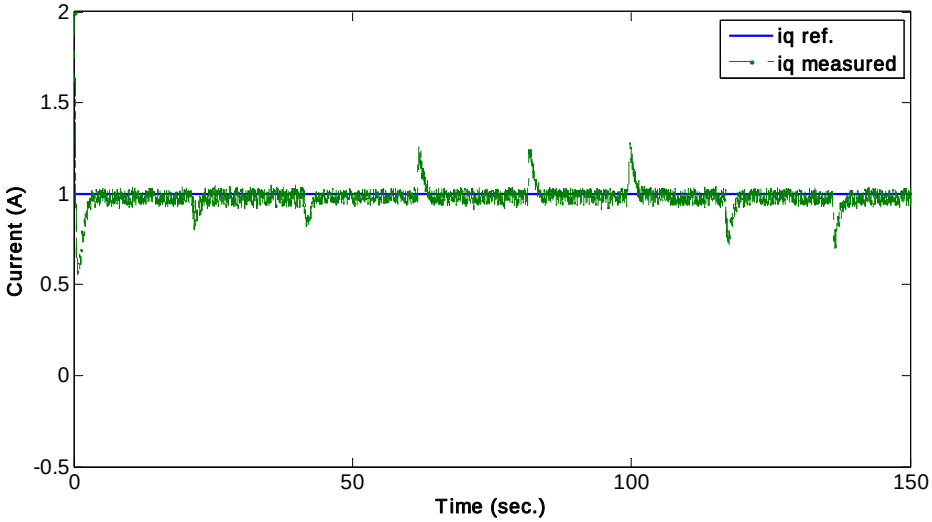

Figure 18. Response of the controlled rotor *q*-current.

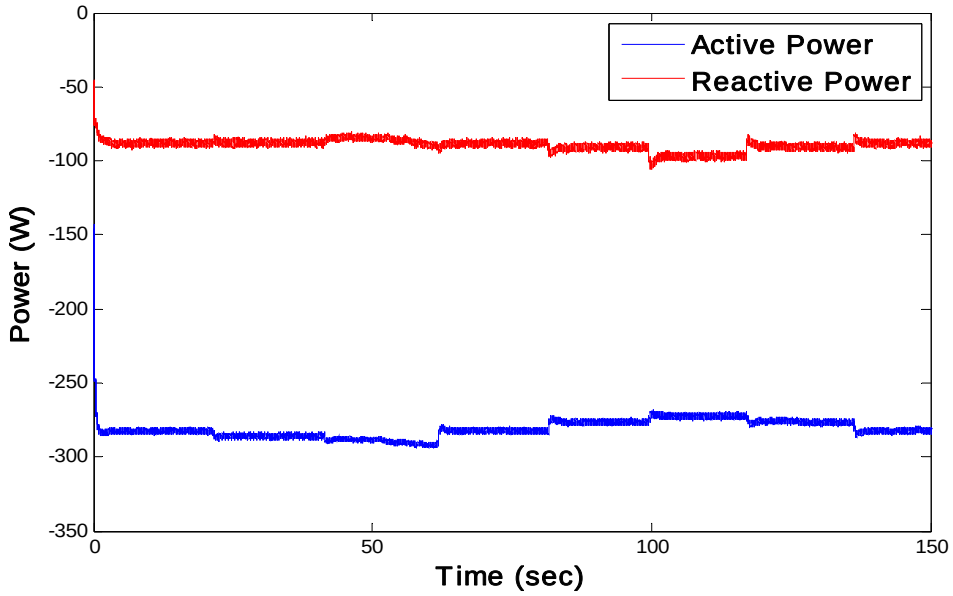

Figure 19. Power response for rotor speed variation.

5. Conclusions

The control of active and reactive power of the studied control scheme for DFIG-based WECS has been achieved under varying rotor speeds. The paper shows the design of the integrated GSC and RSC control, under the direct-current control configuration, to implement the active-reactive power, DC-link voltage, and grid voltage support control functions. Beyond the physical constraints of a DFIG system, the control approach operates the system by regulating the RSC for controlling active and reactive power as the first priority and by controlling the GSC to stabilize the DC-link voltage as the main concern. The experimental results from the laboratory-scale setup are presented to confirm the theoretical analysis of the control system and its application in wind energy conversion systems.

Acknowledgments

This work was supported in part by the Canada Foundation of Innovation (project 30527).

Author Contributions

Aman Tanvir developed the theoretical study of the control system and carried out the experimental implementation. Adel Merabet contributed to the design of the controller and the experimental tests. Rachid Beguenane helped in the real-time simulation and HIL applications.

Conflicts of Interest

The authors declare no conflict of interest.

Appendix

Table A1. System parameters.

Quantity	Value
DFIG machine	
Power	2 kW
Stator voltage	120 V
Rotor voltage	360 V
Stator current	10 A
Rotor current	3.3 A
Speed	1800 RPM
Pole pairs	2
Ls	0.0662
Lr	0.0662
Lm	0.0945
Dynamometer machine	
Required voltage (3 phase)	208 V
Required current (3 phase)	12 A
Speed range	0–3600 RPM
IGBT inverter	
DC-bus voltage	420 V
DC-bus current	10 A
Switching Frequency	0–20 kHz
Grid side controller gains	
Kp = 0.5, Ki = 7, Current regulator = 0.0001 A	
Rotor side controller gains (for idr and iqr)	
Kp = 4.5, Ki = 7.5	

References

1. Abad, G.; Lopez, J.; Rodriguez, M.; Marroyo, L.; Iwanski, G. *Doubly Fed Induction Machine: Modeling and Control for Wind Energy Generation*; El-Hawary, M.E., Ed.; Wiley-IEEE Press: New Jersy, NJ, USA, 2011.
2. Tazil, M.; Kumar, V.; Bansal, R.C.; Kong, S.; Dong, Z.Y.; Freitas, W.; Mathur, H.D. Three-phase doubly fed induction generators: An overview. *Electr. Power Appl. IET* **2010**, *4*, 75–89.
3. Xu, L. Coordinated control of DFIG's rotor and grid side converters during network unbalance. *IEEE Trans. Power Electron.* **2008**, *23*, 1041–1049.
4. Carlson, O.; Hylander, J.; Thorborg, K. Survey of variable speed operation of wind turbines. In Proceedings of the 1996 European Union Wind Energy Conference, Goteborg, Sweden, 20–24 May 1996; pp. 406–409.
5. Zinger, D.S.; Muljadi, E. Annualized wind energy improvement using variable speeds. *IEEE Trans. Ind. Appl.* **1997**, *33*, 1444–1447.
6. DeWind. D8 Series. Brochure. Available online: http://www.dewindco.com (accessed on 30 September 2014).
7. Johnson, G.L. *Wind Energy Systems*; Prentice-Hall: Englewood Cliffs, NJ, USA, 1985.

8. Rabelo, B.; Hofmann, W. Optimal active and reactive power control with the doubly-fed induction generator in the MW-class wind-turbines. In Proceedings of International Conference on Power Electronics and Drives Systems (PEDS), Denpasar, Indonesia, 25 October 2001; Volume 1, pp. 53–58.
9. Tang, Y.; Xu, L. Flexible active and reactive power control strategy for a variable speed constant frequency generating system. *IEEE Trans. Power Electron.* **1995**, *10*, 472–478.
10. Datta, R.; Ranganathan, V.T. Variable-speed wind power generation using doubly fed wound rotor induction machine-a comparison with alternative schemes. *IEEE Trans. Energy Convers.* **2002**, *17*, 414–421.
11. Brune, C.S.; Spee, R.; Wallace, A.K. Experimental evaluation of a variable-speed, doubly-fed wind-power generation system. *IEEE Trans. Ind. Appl.* **1994**, *30*, 648–655.
12. Pena, R.; Clare, J.C.; Asher, G.M. Doubly fed induction generator using back-to-back PWM converters and its application to variable-speed wind-energy generation. *IEEE Proc.-Electr. Power Appl.* **1996**, *143*, 231–241.
13. Cárdenas, R.; Peña, R.; Proboste, J.; Asher, G.; Clare, J. MRAS observer for sensorless control of standalone doubly fed induction generators. *IEEE Trans. Energy Convers.* **2005**, *20*, 710–718.
14. Petersson, A.; Thiringer, T.O.; Harnefors, L.; Petru, T.A. Modeling and experimental verification of grid interaction of a DFIG wind turbine. *IEEE Trans. Energy Convers.* **2005**, *20*, 878–886.
15. Ledesma, P.; Usaola, J. Doubly fed induction generator model for transient stability analysis. *IEEE Trans. Energy Convers.* **2005**, *20*, 388–397.
16. Chowdhury, B.H.; Chellapilla, S. Double-fed induction generator control for variable speed wind power generation. *Electr. Power Syst. Res.* **2006**, *76*, 786–800.
17. Mesbah, M.; Islam, S.; Masoum, M.A.S. A novel direct active power control method for DFIG wind turbine applications. In Proceedings of the IEEE PES Innovative Smart Grid Technologies (ISGT), Hilton Anaheim, CA, USA, 17–19 January 2011.
18. Balogun, A.; Ojo, O.; Okafor, F. Decoupled direct control of natural and power variables of doubly fed induction generator for extended wind speed range using feedback linearization. *IEEE J. Emerg. Sel. Top. Power Electron.* **2013**, *1*, 226–237.
19. Singh, B.; Naidu, N.K.S. Direct power control of single VSC-based DFIG without rotor position sensor. *IEEE Trans. Ind. Appl.* **2014**, *50*, 4152–4163.
20. Zarei, M.E.; Asaei, B. Combined vector control and direct power control methods for DFIG under normal and unbalanced and distorted grid voltage conditions. In Proceedings of the 4th Power Electronics, Drive Systems and Technologies Conference (PEDSTC), Tehran, Iran, 13–14 February 2013; pp. 107–112.
21. Shukla, R.D.; Tripathi, R.K. Speed-sensorless voltage & frequency control in autonomous DFIG based wind energy systems. In Proceedings of the Power Engineering Conference (AUPEC), Perth, Australia, 28 September–1 October, 2014; pp. 1–6.
22. Meegahapola, L.G.; Littler, T.; Flynn, D. Decoupled-DFIG fault ride-through strategy for enhanced stability performance during grid faults. *IEEE Trans. Sustain. Energy* **2010**, *1*, 152–162.
23. Mohammadi, J.; Vaez-Zadeh, S.; Afsharnia, S.; Daryabeigi, E. A combined vector and direct power control for DFIG-Based wind turbines. *IEEE Trans. Sustain. Energy* **2014**, *5*, 767–775.
24. Barambones; Cortajarena, J.A.; Alkorta, P.; de Durana, J.M.G. A real-time sliding mode control for a wind energy system based on a doubly fed induction generator. *Energies* **2014**, *7*, 6412–6433.

25. Xu, L.; Cheng, W. Torque and reactive power control of a doubly fed induction machine by position sensorless scheme. *IEEE Trans. Ind. Appl.* **1995**, *31*, 636–642.
26. Dufour, C.; Belanger, J. Real-time simulation of doubly fed induction generator for wind turbine applications. In Proceedings of the IEEE 35th Annual Power Electronics Specialists Conference, Aachen, Germany, 20–25 June 2004.